

## Electrical and dielectric behavior in blends of polyurethane-based ionomers

C. Tsonos<sup>a</sup>, L. Apekis<sup>a,\*</sup>, K. Viras<sup>b</sup>, L. Stepanenko<sup>c</sup>, L. Karabanova<sup>c</sup>, L. Sergeeva<sup>c</sup>

<sup>a</sup> Physics Department, Faculty of Applied Sciences, National Technical University of Athens, Zografou Campus, GR-15780 Athens, Greece

<sup>b</sup> Physical Chemistry Laboratory, Department of Chemistry, National and Kapodistrian University of Athens, Panepistimioupolis, 15771 Athens, Greece

<sup>c</sup> Institute of Macromolecular Chemistry, National Academy of Sciences of Ukraine, 253160 Kiyev, Ukraine

Received 18 January 2001; accepted 3 April 2001

### Abstract

In the present work, the electrical and dielectric behaviors in ionomer blends of an anion-containing polyurethane (PU<sub>1</sub>) and polyaminourethane (PU<sub>2</sub>) have been investigated by using ac Dielectric Relaxation Spectroscopy (DRS), Differential Scanning Calorimetry (DSC) and Thermally Stimulated Depolarization Currents (TSDC) methods. The ionomer blends are characterized from microphase separation of soft-rich and hard microregions. Two conductivity mechanisms contribute to the dc conductivity of the ionomer blends. That of the shorter relaxation time is correlated to the soft-rich microregions and the other with the longer relaxation time is correlated to the hard microregions. From the comparison between ionomers of different composition, it is found that a faster conductivity relaxation mechanism of the soft-rich microregions implies a faster conductivity relaxation mechanism of the hard microregions. This behavior can be understood in terms of concept of the dynamic energy barriers. From the comparison between the ionomer blends, a smaller temperature difference,  $\Delta T_1 = T_{\text{MWS}} - T_\alpha$ , between the temperatures of the current maximum of the Maxwell–Wagner–Sillars (MWS) and  $\alpha$ -relaxation mechanisms, corresponds to a greater dc conductivity. The formalisms of the dielectric function  $\epsilon^*$ , electric modulus  $M^*$ , and complex impedance  $Z^*$  of the ac dielectric spectroscopy reveal the existence, with different weights, of the various mechanisms of dipolar and conductivity relaxation. The combined use of these formalisms, and especially their imaginary parts, gives the possibility to extract conclusions about the origin and the characteristics of the various relaxation mechanisms, as well as about their correlation with the physical processes which take place in the bulk of the materials. © 2001 Elsevier Science B.V. All rights reserved.

**Keywords:** Polyurethane-based ionomers; Microphase separation; Conductivity relaxation mechanism; MWS mechanism; Dc conductivity

### 1. Introduction

Recently, ionomers and their blends have been under investigation due to the great interest which is both present from the point of view of basic research

in polymer science and from practical point of view of designing new composite materials for advanced technologies [1–8]. Ionomers are polymeric materials in which ionic or effective groups are attached in the structure of their macromolecules.

The ion-containing segmented polyurethanes and their blends are an important category of ionomers because of the elastomeric and thermoplastic properties of these materials. The segmented polyurethanes

\* Corresponding author. Tel.: +30-1-772-2990; fax: +30-1-772-2932, +30-1-772-3025.

E-mail address: lapekis@central.ntua.gr (L. Apekis).

are linear copolymers in which the general structure of their macromolecules has the form  $(A-B)_n$ , where A is the soft (SFT) segment and B is the stiff (STF) segment. In polyurethane-based ionomers, the ionic groups are usually attached to the structure of STF segments. The main difference between segmented polyurethanes and ion-containing segmented polyurethanes is the structure of the hard microdomains [9]. In polyurethane system non-containing ionic groups, the microphase separation (degree of microphase separation, DMS) is the result of the arrangement of the hard segments into microdomains with enhanced order, due mainly to hydrogen bonds. In the ion-containing segmented polyurethanes, to this arrangement additional electrostatic interactions contribute, due to the presence of the ionic groups, which in these materials are usually located at the hard segments of the macromolecules. When the weight fraction of the soft phase is higher than that of the hard phase, then soft phase can be considered as the continuous phase into which the hard microdomains are dissolved, forming a 'three-dimensional lattice' [10,11].

Introducing ion-groups into polyurethane-polymers with a highly developed network of physical bonds provides an additional 'ionic network'. This defines, to a great extent, structural and other properties of these systems. It has been previously shown [12,13] that the introduction of the ion-groups into one of the components of similar chemical nature (polyurethane–polyurethane IPNs) leads to significant changes of its microphase structure [12] and adhesive properties [13].

In a previous work, two-component blends based on polyurethanes containing ion and other active groups were investigated [22]. Dielectric Relaxation Spectroscopy (DRS), Differential Scanning Calorimetry (DSC), and small angles X-ray scattering (SAXS) were used in a study of the molecular mobility and microphase morphology and their dependence on the composition of these ionomers. The investigation was carried out in the low temperature region, 77–300 K. Based on TSDC measurements, a parameter  $m_{\text{TSDC}}$ , as a criterion expressing a relative degree of phase mixing, is introduced [22].

In the present work, we continue the investigation on two-component blends of polyurethane-based ionomers in a higher temperature region, 300–473

K, by means mainly of ac dielectric spectroscopy and Thermally Stimulated Depolarization Current methods (TSDC), and Differential Scanning Calorimetry (DSC) measurements. In this work, we study the correlation of the electrical and dielectric behavior with the micromorphology of the ionomer blends.

## 2. Materials and experimental methods

### 2.1. Materials

Oligooxytetramethylenglycol (OTMG) MW = 1000 was dried at 90°C in 1 mm Hg vacuum for 48 h before use. *P*-hydroxy-benzoic acid (HBA) was purified by recrystallization from water. *N*-methyl-diethanolamine (NMDA) and dimethylformamide (DMF) were distilled before use. Toluylene-diisocyanate (a mixture of 2.4:2.6 isomers in the ratio 65:35) (TDI) and magnesium oxide (MgO) of pure grade were used without further purification.

#### 2.1.1. Preparation of magnesium salt of HBA (Mg-HBA)

The reaction between HBA (2 M) and MgO (1 M) was carried out in solution (isopropanol or acetone) at 60°C. After the reaction, the product was filtered and was washed with acetone several times. Then it was dried in vacuum at 60°C.

#### 2.1.2. Preparation of linear polyurethanes

Preparation of the polyurethane prepolymer (PP). The isocyanate-terminated PP was prepared by reacting 2 equiv of TDI with 1 equiv of OTMG 1000 as described [14].

The anion-containing polyurethane (PU<sub>1</sub>) and polyaminourethane (PU<sub>2</sub>) were prepared in DMF by mixing 1 equiv of PP with 1 equiv of Mg-HBA (for the PU<sub>1</sub>) or NMDA (for the PU<sub>2</sub>) at room temperature.

The final concentration of PU-solutions was about 20%. The mixtures were placed in teflon moulds. After drying at room temperature, the samples were heated at 85°C for 48 h. Molecular weight of PU was defined by viscosimetry method and has the value: MW of PU<sub>1</sub> = 50 000–60 000 and MW of PU<sub>2</sub> = 20 000–25 000.

### 2.1.3. Preparation of polymer blends based on $PU_1$ and $PU_2$

The polymer blends were prepared by the following way. The PP and Mg-HBA were added to the solution containing  $PU_2$  in DMF. The components were mixed for 30–40 s with a high-torque stirrer at room temperature. The mixture was placed in teflon molds, dried at room temperature, and then was heated at 85°C for 48 h. Thus, polymer blends containing 5%, 10%, 30% and 50% of  $PU_1$  were obtained. The samples were in the form of sheets and were cylinders of 0.10–0.60 mm thickness.

## 2.2. Experimental methods

### 2.2.1. Alternating current (ac) dielectric measurements

ac dielectric measurements, in the frequency range  $10^0$ – $10^6$  Hz, were carried out using a Schlumberger frequency response analyzer (FRA 1260) supplemented with a buffer amplifier of variable gain. A two-terminal parallel-plate capacitor dielectric cell with gold-plated metal electrodes (Novocontrol) was used in combination with an Ando type TO-19 thermostatic oven. Prior to ac dielectric measurements, the samples were heated to 340 K for 2 days to minimize the concentration of the moisture. We performed complex admittance measurements, and the temperature of measurements was varied in the range 323–413 K with an accuracy better than  $\pm 0.1$  K.

### 2.2.2. Thermally Stimulated Depolarization Currents (TSDC) measurements

We used a common experimental apparatus for TSDC measurements in the temperature of 77–300 K [15]. The standard electrodes of the measuring capacitor were made of brass. Typical experimental conditions were 5 kV/cm for the polarizing field, 298 K for the polarization temperature, 5 min for polarizing time, 7 K/min for the cooling rate and 3–4 K/min for heating rate. The uncertainty for the peak temperatures,  $T_m$ , was  $\pm 1$  K.

### 2.2.3. Differential Scanning Calorimetry (DSC) measurements

Differential Scanning Calorimetry measurements were carried out at the temperature range 300–473 K by using a Perkin-Elmer DSC-4. The samples mass

were 10–20 mg, while the heating rate was 20 K/min.

## 3. Experimental results and discussion

### 3.1. Differential Scanning Calorimetry (DSC) measurements

In order to study the thermal behavior of the  $PU_1/PU_2$  ionomer blends, DSC measurements were carried out at the temperature range of 300–473 K.

In Fig. 1, DSC thermograms, regarding the ionomers  $PU_1/PU_2$  in the region of high temperatures, 300–473 K, are displayed. Endothermic peaks are observed in the 350–380-K temperature range. The existence of these peaks is attributed to the disordering of the hard microdomains [16,17]. Due to their disordering, these microdomains are characterized by increased mobility, and thus become softer. The fact that the endothermic peak temperatures of ionomers  $PU_1/PU_2$  were found to be a few dozens of degrees K higher than the respective temperature of non-ionic segmented polyurethanes [18,19] may be attributed to the existence of ionic and effective groups in the hard segments of  $PU_1$  and  $PU_2$ , in the sense that at stronger electrostatic interactions between the ionic groups, a greater thermal energy is required to observe the respective disorderings.

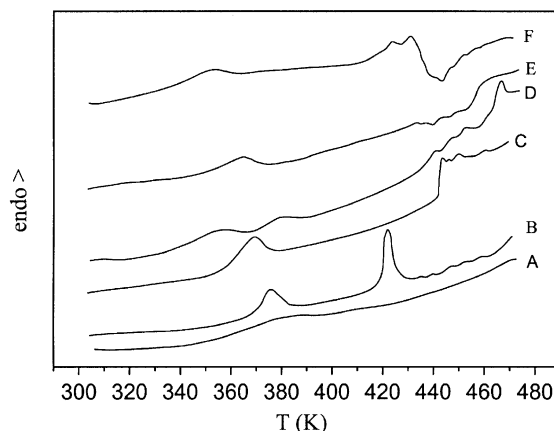


Fig. 1. DSC thermograms for the  $PU_1/PU_2$  (%) ionomers: A (100/0), B (50/50), C (30/70), D (10/90), E (5/95), F (0/100).  $dH/dt$  values are in arbitrary units different for each ionomer, and the curves have been shifted to appear in the figure.

The endothermic peaks, which are displayed for the ionomer 10/90 in the temperature of 350 and 370 K, were derived possibly from hard microregions with different composition (hard microregions where the component  $PU_1$  or  $PU_2$  is prominent).

The melting peak, which is displayed for the ionomer 50/50 in the temperature of 413 K, may be derived from the melting of well-organized microcrystallites of hard microregions [17]. All the other ionomers do not display a respective melting peak. The successive irregular small endothermal peaks, which are shown in thermograms of the ionomers, except 100/0, for temperatures higher than 420 K, may be attributed from changes in the contact-surface between sample and cell. Immediately following the DSC thermograms, at 473 K, all the ionomers studied, except 100/0, had been in fluid state. This fact probably implies that hard microregions, which ensured the satisfactory mechanical behavior of these ionomers, had been completely dissolved into the soft phase. The ionomer 100/0 exhibited the best thermal stability at 473 K.

In a previous work, we studied the molecular mobility and microphase morphology and their dependence on the composition of the same ionomer blends [22].  $PU_1$  (100/0) ionomer has a high degree of microphase separation. The introduction of  $PU_2$  (0/100) in the blends causes defects in the hard domains and leads to a structure with mixing of the soft and hard microphases. As a result of the complexity of the  $PU_1/PU_2$  ionomer systems, their structure and their properties are not simple functions of their composition. The classification of the investigated ionomer blends in order of decreasing phase mixing ( $PU_1/PU_2$  in %) is 50/50 (mixed) > 0/100 > 5/95 > 10/90 > 100/0 > 30/70 (high separation) [22].

### 3.2. Dielectric Relaxation Spectroscopy (DRS) measurements

The dielectric data have been analyzed and discussed by using different functions of the dielectric spectroscopy as, the dielectric function  $\epsilon^*$ , the complex impedance  $Z^*$  and the electric modulus  $M^*$ . The dielectric function  $\epsilon^*$  usually is used to describe the dielectric behavior (polarization mechanisms) of the materials. On the other hand, the

complex impedance  $Z^*$  and the electric modulus  $M^*$  usually are used to describe the electrical behavior (conductivity relaxation mechanisms) of the materials.

#### 3.2.1. The Maxwell–Wagner–Sillars (MWS) mechanism in the dielectric function formalism $\epsilon^*$

In the dielectric function formalism,  $\epsilon^*$ , all the  $PU_1/PU_2$  ionomer blends exhibit similar spectra in the temperature range of 323–413 K. Two contributions are present, one from a relaxation mechanism and another from the dc conductivity.

In Fig. 2, the dependence of the real ( $\epsilon'$ ) and imaginary part ( $\epsilon''$ ) of dielectric function ( $\epsilon^*$ ) on the frequency ( $f$ ) of the ionomer 30/70, for various

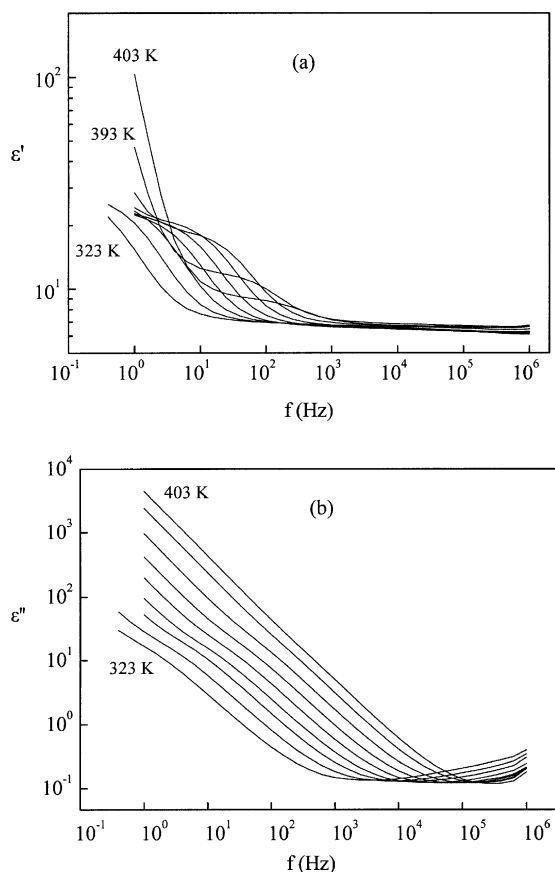


Fig. 2. The real part  $\epsilon'$  (a) and the imaginary part  $\epsilon''$  (b) of the dielectric function  $\epsilon^*$  versus the frequency  $f$  for the ionomer 30/70 at several temperatures: 323, 333, 343, 353, 363, 373, 383, 393, 403 K.

temperatures, is shown. In the plot of  $\log \varepsilon'$  versus  $\log f$  (Fig. 2a), a mechanism of dielectric losses is evidently shown, which is shifted to higher frequencies as the temperature increases. The contribution of this mechanism to the real part ( $\varepsilon'$ ) of dielectric function is fairly significant ( $\sim 10$ ) in the region of lower temperature, whereas in the region of high temperature ( $T > 370$  K), it decreased abruptly. The great value of this contribution to  $\varepsilon'$  (great losses) implies that the above mechanism does not have a dipolar origin but it is related to charge (ion) migration in the interior of the ionomer. Considering the fact that the micromorphology of the ionomer is heterogenous (microphase separation), this relaxation mechanism should correspond to MWS-relaxation mechanism, which develops between hard/soft/hard (STF/SFT/STF) microregions. The MWS-relaxation is due to interfacial polarization related to ion migration and the existence of soft and hard microdomains with different conductivity [20–22].

In the region of higher temperatures and low frequencies, an abrupt increase of  $\varepsilon'$  values has been observed which is related with electrode polarization effects. At low frequencies and high temperatures, due to higher conductivity, charges are concentrated at the electrodes–sample interfaces [23]. The increase in  $\varepsilon'$  values, in the respective frequency region, is attributed to the contribution of capacities that are correlated with the electrodes–sample interfaces, and characterized by far higher values in relation to the bulk capacities of the samples.

In Fig. 2b, which displays the dependence of  $\varepsilon''$  from frequency,  $f$ , for various temperatures, the MWS mechanism is distinct only in the region of lower temperatures, where the contribution of dc conductivity in the dielectric losses is not dominant. The contribution of the dc conductivity to the dielectric losses,  $\varepsilon''$ , is inversely proportional to frequency  $f$ , i.e. corresponds to the linear segment of lower frequencies in the  $\log \varepsilon''$  versus  $\log f$  plots. In the region of higher temperatures, the contribution of dc conductivity is prominent, and therefore, overwhelms the mechanism of interfacial polarization. At the higher frequencies, a relaxation mechanism contributes to the  $\varepsilon''$  versus  $\log f$  spectra. This mechanism corresponds to the  $\alpha$ -relaxation mechanism of the soft-rich microphases, which was extensively investigated and analyzed in our previous work [22].

The respective diagrams, i.e.  $\log \varepsilon'$  and  $\log \varepsilon''$  versus  $\log f$ , of the other ionomers in the same temperature range, resemble those of ionomer 30/70 (Fig. 2a,b). In the diagrams  $\log \varepsilon''$  versus  $\log f$ , fittings of the following empirical equation has been accomplished:

$$\varepsilon'' = A \omega^{-s} + \frac{\Delta \varepsilon' \sin(\beta \varphi)}{[1 + 2(\omega \tau_0)^{1-\alpha} \sin(0.5\pi\alpha) + (\omega \tau_0)^{2(1-\alpha)}]^{1/\beta}} \quad (1)$$

where

$$\varphi = \arctan \left[ \frac{(\omega \tau_0)^{1-\alpha} \cos(0.5\pi\alpha)}{(1 + (\omega \tau_0)^{1-\alpha} \sin(0.5\pi\alpha))} \right].$$

The first term of Eq. (1) describes the contribution of the dc conductivity to the  $\varepsilon''$  losses.  $A$  and  $s$  are parameters and  $\omega$  is the angular frequency,  $\omega = 2\pi f$  [24]. Parameter  $A$  is related with the value of the material's conductivity  $\sigma$  according to the equation  $A = \sigma/\varepsilon_0$ , where  $\varepsilon_0$  is the dielectric constant of empty space.

The second term of the Eq. (1) is the empirical equation of Havriliak–Negami (H–N) [25] and describes the contribution of the MWS—dielectric mechanism to the dielectric losses,  $\varepsilon''$ . Parameters  $\alpha$  ( $0 \leq \alpha < 1$ ) and  $\beta$  ( $0 < \beta \leq 1$ ) depict the symmetrical and asymmetric deviation from simple relaxation time, respectively. When  $\alpha = 0$  and  $\beta = 1$ , the H–N equations of  $\varepsilon'$ ,  $\varepsilon''$  coincide with the respective Debye equations.  $\Delta \varepsilon'$  is the contribution of the MWS mechanism to the real part of the dielectric function  $\varepsilon^*$  and  $\tau_0$  ( $= 1/2\pi f_0$ ) is a time parameter closely correlated with the maximal frequency  $f_{\max}$  of the dielectric losses,  $\varepsilon''$ .

In Fig. 3, the best fit of Eq. (1) on a diagram  $\log \varepsilon''$  versus  $\log f$  concerning the ionomer 30/70 at 373 K is shown representatively. In the same figure, the contributions of the conductivity and of the MWS mechanism to the dielectric losses  $\varepsilon''$  are also displayed. From the values of parameter  $\tau_0$  regarding the best fit of Eq. (1) on the diagrams  $\log \varepsilon''$  versus  $\log f$  of all ionomers studied in the respective temperatures measured, the frequencies of  $f_{\max, \varepsilon''}$ , which correspond to the maximum values of  $\varepsilon''$  dielectric losses of MWS mechanisms are derived.

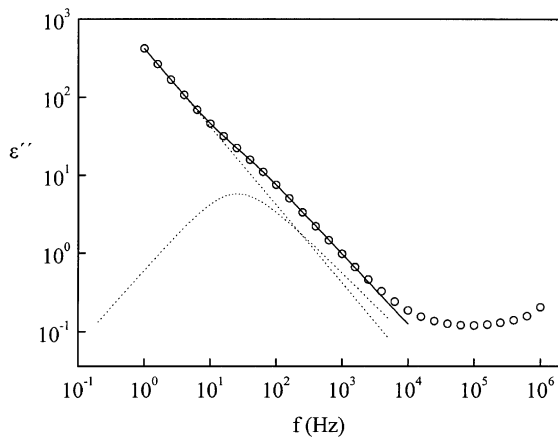


Fig. 3. The imaginary part  $\varepsilon''$  of the dielectric function  $\varepsilon^*$  versus frequency  $f$  of the ionomer 30/70 at 373 K. The solid line is the best fit according to Eq. (1). The dotted lines show the contribution of the dc conductivity and MWS relaxation to the dielectric losses  $\varepsilon''$ . The values of the parameter are:  $A = 2623.36$ ,  $s = 1.00$ ,  $\alpha = 0.06$ ,  $\beta = 0.88$ ,  $\Delta\varepsilon' = 13.32$  and  $f_0 (= 1/2\pi\tau_0) = 22.90$ .

In Fig. 4, the correlation of  $\log f_{\max, \varepsilon''}$  with reciprocal temperature (Arrhenius plots) is shown. A change in the slope of the Arrhenius diagrams is observed in the temperature region of 350–380 K. This change may be related with the disordering of hard microregions in the respective temperature regions (Fig. 1). The activation energies  $E$  of MWS mechanisms, in these temperature regions before and

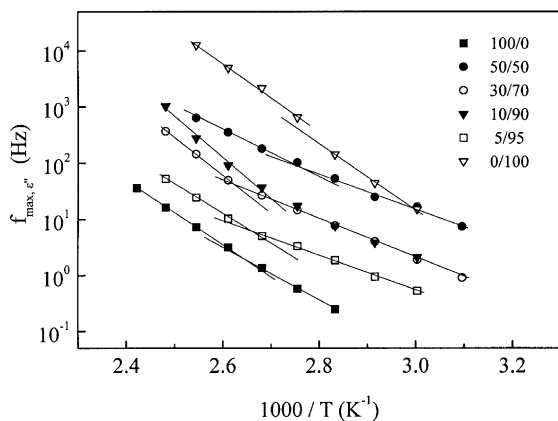


Fig. 4. Arrhenius plot of the frequency of the maximum of the  $\varepsilon''$  ( $f$ ) peak related to the MWS relaxation,  $f_{\max, \varepsilon''}$ , for all ionomers  $\text{PU}_1/\text{PU}_2$ .

Table 1

The activation energies  $E_1$ ,  $E_2$  of the MWS mechanisms relaxation time, for the temperatures lower and higher, respectively, than the characteristic endothermic peak temperatures of the DSC thermograms

$\text{PU}_1/\text{PU}_2$	100/0	50/50	30/70	10/90	5/95	0/100
$E_1$ (eV)	0.96	0.65	0.70	0.72	0.64	1.14
$E_2$ (eV)	1.07	0.80	1.34	1.44	1.03	1.20

after the respective changes to the slope of the Arrhenius diagrams regarding ionomers  $\text{PU}_1/\text{PU}_2$ , have been calculated by the best fit of the Arrhenius equation:

$$f_{\max} = f_0 \exp\left(-\frac{E}{kT}\right). \quad (2)$$

In the above equation,  $f_0$  is a pre-exponential parameter,  $E$  is the activation energy of MWS mechanism,  $k$  is the Boltzmann constant and  $T$  is the absolute temperature. The values of  $E$  of MWS mechanisms are shown in Table 1.

In Fig. 5, the contribution of the MWS mechanisms to the real part of the dielectric function  $\Delta\varepsilon'$  as a function of temperature is displayed. The values of  $\Delta\varepsilon'$  are those that have been derived from the best contributions of the Eq. (1) on the diagrams  $\log\varepsilon''$  versus  $\log f$  of the  $\text{PU}_1/\text{PU}_2$  ionomers. For all ionomers, except 100/0, a drastic decrease of  $\Delta\varepsilon'$  is observed which is correlated with tempera-

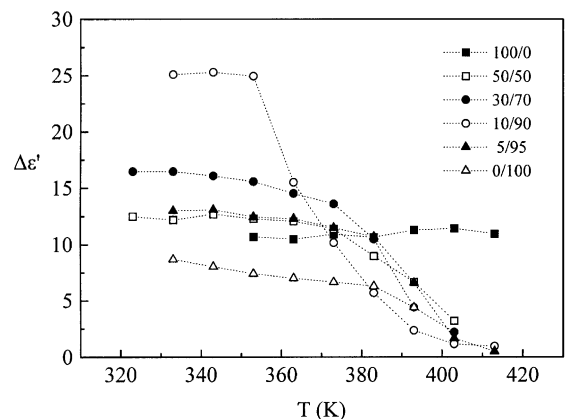


Fig. 5. The contributions to the real part  $\varepsilon'$  of the dielectric function  $\varepsilon^*$ ,  $\Delta\varepsilon'$ , of the MWS relaxation, as a function of temperature  $T$ , for all ionomers  $\text{PU}_1/\text{PU}_2$ .

tures increase, and appear in the same temperature region where the endothermic peaks of DSC thermograms are observed (Fig. 1). This significant decrease of  $\Delta\varepsilon'$ , which is correlated with the temperature increase, is attributed to the disordering of the hard microregions. Subsequent to the disordering of hard microregions, the mobility of hard segments increases gradually by increasing temperature, which results in the loosening of intermolecular interactions (hydrogen bonds and electrostatic nature interactions). Regarding the ionic segmented polyurethanes, subsequent to the softening of the hard microregions at 330–350 K, a gradual dissolution of hydrogen bonds between the hard segments takes place which is correlated to the temperature increase [17]. The gradual increase in the mobility of hard segments, due to the loosening of their intermolecular interactions, will induce a gradual decrease in the difference between specific resistance values ( $\rho$ ) of soft and hard microregions, respectively. Therefore, after the disordering of hard microregions due to the temperature increase, a gradual decrease in interfacial polarization, which takes place between STF/SFT/STF microregions, and consequently, a gradual  $\Delta\varepsilon'$  decrease of the MWS mechanisms, is expected.

The fact that there is no decrease in  $\Delta\varepsilon'$  of ionomer 100/0, in the respective temperature region, is attributed to the great difference between the specific resistance value of hard microregions compared with the respective value of soft ones, as it is going to be shown afterwards. In this temperature region, immediately after the disordering of its hard microregions, despite the gradual increase in the mobility of the respective hard segments, the difference of specific resistance between soft and hard microregions remains great, and due to this fact, no  $\Delta\varepsilon'$  decrease is observed.

### 3.2.2. The two conductivity relaxation mechanisms in the complex impedance formalism $Z^*$

In the complex impedance formalism  $Z^*$  ( $= 1/2\pi fC_0\varepsilon^*$ ) and specifically  $Z''$  spectra versus  $\log f$  of all ionomers PU<sub>1</sub>/PU<sub>3</sub>, two overlapping conductivity relaxation mechanisms are observed, which are shifted to higher frequencies in relation to temperature rise. On the diagrams  $Z''$  versus  $\log f$  of all ionomers, in a complete range of temperatures, there has been a fitting to a theoretical curve which com-

prises a sum of two Cole–Cole equations regarding the imaginary part of complex impedance  $Z''$ , in analogy to the equation for  $\varepsilon''$  [25,26]:

$$Z'' = \sum_{i=1}^2 \frac{\Delta Z'_i ((\omega\tau_{0i})^{1-\alpha_i} \cos(0.5\pi\alpha_i))}{1 + 2(\omega\tau_{0i})^{1-\alpha_i} \sin(0.5\pi\alpha_i) + (\omega\tau_{0i})^{2(1-\alpha_i)}} \quad (3)$$

$\Delta Z'_i$  is the contribution of each conductivity relaxation mechanism to the real part of complex impedance, i.e. the contribution of each mechanism to the total impedance of the material,  $\Delta Z'_i = R_i$ . The contribution to the material's impedance of the dipolar mechanisms, which reconstitute at higher temperatures, is regarded insignificant.  $\omega$  is the angular frequency,  $\alpha_i$  is a parameter which is correlated with the mean width of the curve of each mechanism and obtains values of  $0 \leq \alpha < 1$ . The conductivity mechanism is described by a simple relaxation time in case that  $\alpha = 0$ , while when  $\alpha > 0$ , this mechanism is described by symmetrical distribution of relaxation times. The parameter  $\tau_{0i}$  ( $= 1/2\pi f_{0i}$ ) describes the mean relaxation time of each conductivity relaxation mechanism and corresponds to the frequency of maximum  $Z''$  value.

In Fig. 6, a representative diagram  $Z''$  versus  $\log f$  of the ionomer 30/70 with the respective fitting of

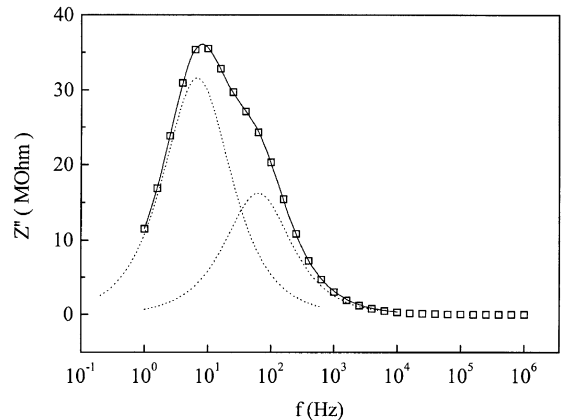


Fig. 6. The imaginary part  $Z''$  of the complex impedance  $Z^*$  versus frequency  $f$  of the ionomer 30/70 at 363 K. The solid line is the best fit according to Eq. (3). The dotted lines show the contribution of the two conductivity relaxation mechanisms to the  $Z''$ . The values of the parameter are:  $\alpha_1 = 0.06$ ,  $\Delta Z'_1 = 69.52$ ,  $f_{01} (= 1/2\pi\tau_{01}) = 6.79$ ,  $\alpha_2 = 0.05$ ,  $\Delta Z'_2 = 35.35$ ,  $f_{02} (= 1/2\pi\tau_{02}) = 62.65$ .

Eq. (3) is displayed. In the same figure, the contributions of two conductivity mechanisms, i.e. the mechanism of low frequencies (l.f.) and the mechanism of high frequencies (h.f.), are also distinct.

In Fig. 7, the Arrhenius diagrams,  $\log f_{\max, Z''}$  versus  $1/T$ , of the two conductivity mechanisms regarding all ionomers are depicted. Changes are observed in the slopes of these diagrams at temperature region 350–380 K, and this fact implies that the disordering (softening) of the hard microregions affects the two conductivity mechanisms. In Table 2, the values of activation energies  $E_{Zh1}$ ,  $E_{Zh2}$ ,  $E_{Zl1}$  and  $E_{Zl2}$ , which have been derived from the best fits of the respective Arrhenius equation  $f_{\max, Z''} = f_0 \exp(-E/kT)$  (Eq. (2)), are shown. Indexes h and l

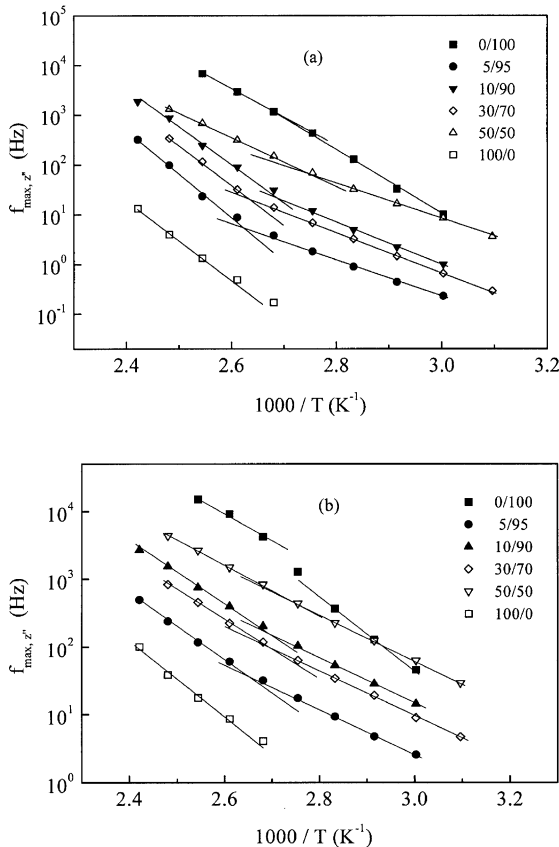


Fig. 7. Arrhenius plot,  $\log f_{\max, Z''}$  versus  $1000/T$ , of the: lower frequencies (l.f.) conductivity relaxation (a), and higher frequencies conductivity relaxation (b), for all PU<sub>1</sub>/PU<sub>2</sub> ionomers.

Table 2

The activation energies  $E_{Zl}$ ,  $E_{Zh}$  of the (l.f.) and (h.f.) conductivity mechanisms relaxation time  $\tau_z (= 1/2\pi f_{\max, Z''})$ , for the temperatures lower (1) and higher (2), respectively, than the characteristic endothermic peak temperatures of the DSC thermograms

PU <sub>1</sub> /PU <sub>2</sub>	100/0	50/50	30/70	10/90	5/95	0/100
$E_{Zl1}$ (eV)	–	0.70	0.80	0.85	0.72	1.29
$E_{Zl2}$ (eV)	1.57	0.95	1.57	1.42	1.66	1.14
$E_{Zh1}$ (eV)	–	0.67	0.70	0.69	0.67	1.06
$E_{Zh2}$ (eV)	1.23	0.72	0.87	0.88	0.96	0.80

symbolize the conductivity mechanisms of high and low frequencies, respectively, whereas the indexes 1 and 2 symbolize the temperature region before and after the disordering of the hard microregions, respectively. From the values of Table 2, it can be concluded that  $\Delta E_{Zl} = \Delta E_{Zl2} - \Delta E_{Zl1}$  changes of the (l.f.) conductivity mechanisms are greater than the respective changes  $\Delta E_{Zh} = \Delta E_{Zh2} - \Delta E_{Zh1}$  of the (h.f.) conductivity mechanisms of ionomers, except 0/100. As mentioned, PU<sub>1</sub>/PU<sub>2</sub> are characterized by microphases separation [22]. Thus, the two conductivity relaxation mechanisms should be correlated with the soft and hard microregions of the PU<sub>1</sub>/PU<sub>2</sub> ionomers. The characteristic disordering, in the temperature range 350–380 K, induces greater structural and mobility changes to the hard microregions and therefore, it is expected to have greater influence to the conductivity mechanism which is correlated with these regions. As shown in Table 2, the disordering to the hard microregions has a systematically greater influence on (l.f.) conductivity mechanism (except 0/100), this mechanism should be correlated with the hard microregions of ionomers PU<sub>1</sub>/PU<sub>2</sub>.

DSC measurements have shown infrequently small alteration regarding the specific heat  $\Delta C_p$  of 0/100 during the glass transition of the soft microphases [22]. This fact has been attributed to the restriction of the mobility of a significant amount of soft segments occurring in the boundary regions around the hard microdomains [22]. Thus, it is possible that the different behavior of activation energies  $E_{Zh}$  and  $E_{Zl}$  of the two conductivity mechanisms regarding 0/100 (Table 2) may be correlated with the individuality of SFT/STF interfaces of the particular ionomer.

### 3.2.3. The two conductivity relaxation mechanisms in the electric modulus formalism $M^*$

Regarding the formalism of electric modulus  $M^*$  ( $= 1/\varepsilon^*$ ), in all ionomers PU<sub>1</sub>/PU<sub>2</sub>, two overlapping mechanisms are observed, which are shifted to higher frequencies when the temperature increase. These mechanisms correspond to (l.f.) and (h.f.) conductivity mechanisms as it is going to be shown afterwards. On diagrams  $M''$  versus  $\log f$ , of all ionomers, a fitting has been accomplished to a theoretical curve that comprises a sum of two Cole–Cole equations regarding the imaginary part of electric modulus  $M''$ , in analogy to the equation for  $\varepsilon''$  [25,26]:

$$M'' = \sum_{i=1}^2 \frac{\Delta M'_i ((\omega\tau_{0i})^{1-\alpha_i} \cos(0.5\pi\alpha_i))}{1 + 2(\omega\tau_{0i})^{1-\alpha_i} \sin(0.5\pi\alpha_i) + (\omega\tau_{0i})^{2(1-\alpha_i)}} \quad (4)$$

$\Delta M'_i$  is the contribution of each conductivity mechanism to the real part of electric modulus.  $\omega$  is the angular frequency,  $\alpha_i$  is a parameter which is correlated to the mean curve width of each mechanism and taking values  $0 \leq \alpha < 1$ . The parameter  $\tau_{0i}$  ( $= 1/2\pi f_{0i}$ ) describes the mean relaxation time of each conductivity mechanism in  $M^*$  formalism and corresponds to the frequency of maximum  $M''$  value.

In Fig. 8, the diagram  $M''$  versus  $\log f$  with the respective best fit of Eq. (4), regarding ionomer 50/50, is shown representatively.

### 3.2.4. A comparison between the functions $\varepsilon^*(f)$ , $M^*(f)$ and $Z^*(f)$ of the dielectric spectroscopy

The equivalent circuit of a conductivity mechanism with a single relaxation time ( $\alpha = 0$  in Eq. (4)) corresponds to the parallel combination of resistance  $R$  and capacity  $C$  [23]. The maximum  $M''$  value is defined by:

$$M''_{\max} = \frac{C_0}{2C} \quad (5)$$

where  $C_0$  is the geometric capacity of the free space and  $C$  is the value capacity of conductivity mechanism, i.e. the capacity which corresponds to the conductive channels of the respective mechanism.

In the  $M^*$  formalism, besides the conductivity mechanisms, the polarization mechanisms are also registered. This is because the capacities that corre-

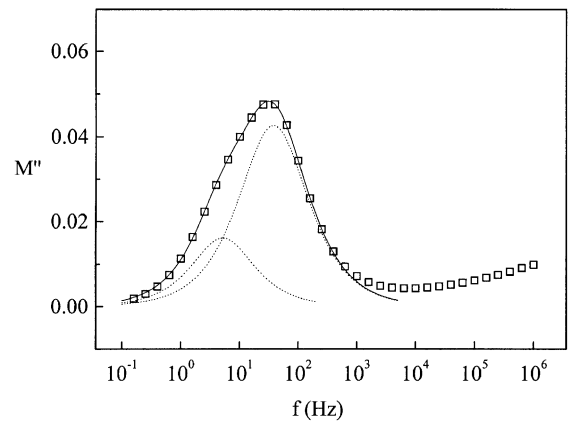


Fig. 8. The imaginary part  $M''$  of the electric modulus  $M^*$  versus frequency  $f$  of the ionomer 50/50 at 323 K. The solid line is the best fit according to Eq. (4). The dotted lines show the contribution of the two conductivity relaxation mechanisms to the  $M''$ . The values of the parameters are:  $\alpha_1 = 0.06$ ,  $\Delta M'_1 = 0.035$ ,  $f_{01} (= 1/2\pi\tau_{01}) = 5.18$ ,  $\alpha_2 = 0.12$ ,  $\Delta M'_2 = 0.103$ ,  $f_{02} (= 1/2\pi\tau_{02}) = 37.76$ .

spond to the polarization mechanisms,  $C_{\text{dip}} = C_0 \Delta \varepsilon' = C_0 (\varepsilon_s - \varepsilon_\infty)$ , usually do not differ significantly from the capacities which correspond to the conductivity relaxation mechanisms,  $C_{\text{cond}} = C_0 \varepsilon_s$ , for the same materials ( $\Delta \varepsilon' = \varepsilon_s - \varepsilon_\infty \approx \varepsilon_s$ ). As it can be assessed by Eq. (5), on the diagrams  $M''$  versus  $\log f$ , the most prevalent mechanisms will be those with the minimum volume capacities. The strong capacity phenomena of electrode–material interfaces, are vanished within  $M^*$  formalism.

In contrast to  $M^*$  formalism, in the complex impedance formalism  $Z^*$ , the magnitude of a conductivity mechanism,  $Z''_{\max}$ , does not depend on the volume capacity but on the resistance  $R$  [27]:

$$Z''_{\max} = \frac{R}{2} \quad (6)$$

where  $R$  is the resistance which corresponds to the conductivity relaxation mechanism. On diagrams  $Z''_{\max}$  versus  $\log f$ , those mechanisms with the maximum resistance will be prevalent. Due to the fact that the volume resistance of conductivity mechanisms is far greater than the respective one of dipolar mechanisms, these mechanisms will be prevalent on the diagrams  $Z''_{\max}$  versus  $\log f$ .

The formalism of dielectric function  $\varepsilon^*$  exhibits only polarization mechanisms (dipolar, MWS) and records the contribution of dc conductivity. However, the use of  $\varepsilon^*$  formalism cannot distinguish the existence of various conductivity mechanisms which occur into the material and contribute to the dc conductivity.

The volume capacities of the conductivity mechanisms usually do not have strong dependence on temperature [28]. Thus, when two conductivity mechanisms with no very different relaxation times are characterized by significant difference in volume capacity, it is extremely difficult to detect both of them within  $M^*$  formalism simultaneously. The resistances of the conductivity relaxation mechanisms are quite sensitive to temperature changes (thermally activated conductivity). Thus, in the case of two mechanisms having no very different relaxation time, it is likely that they will be detected simultaneously in  $Z^*$  formalism, within a wide temperature range.

The maximum frequencies regarding the values  $\varepsilon''$ ,  $M''$  and  $Z''$  of the same physical process follow the sequence  $f_{\max, M''} \geq f_{\max, Z''} > f_{\max, \varepsilon''}$  [29]. When the physical process is correlated to charge migrations within long distances (long range conductivity relaxation process), which is characterized by a single relaxation time (parameter Cole–Cole  $\alpha = 0$ ), then  $f_{\max, M''} = f_{\max, Z''}$  [29,30]. When there is distribution of relaxation times ( $\alpha > 0$ ), then  $f_{\max, M''} > f_{\max, Z''}$ . When the distribution of relaxation times is narrower ( $\alpha \approx 0$ ), then  $f_{\max, M''} \approx f_{\max, Z''}$  [30].

When a physical process is described by a single relaxation time,  $\tau_\varepsilon$ , in the  $\varepsilon^*$  formalism, then in the  $M^*$  formalism the relaxation time,  $\tau_M$ , is given by:

$$\tau_M = \frac{\tau_\varepsilon}{\frac{\Delta \varepsilon' + \varepsilon_\infty}{\varepsilon_\infty}} \quad (7)$$

where  $\varepsilon_\infty$  is value of real part of dielectric function  $\varepsilon'$  in high frequencies and  $\Delta \varepsilon'$  is the contribution of this physical process to  $\varepsilon'$  [29]. When a physical process is described by a symmetrical distribution of relaxation time (behavior Cole–Cole,  $\beta = 1$ ) within the  $\varepsilon^*$  formalism, with mean relaxation time  $\tau_\varepsilon =$

$1/2\pi f_{\max, \varepsilon''}$ , then within formalism  $M^*$  the respective  $\tau_M$  is defined by:

$$\tau_M = \frac{\tau_\varepsilon}{\left( \frac{\Delta \varepsilon' + \varepsilon_\infty}{\varepsilon_\infty} \right)^{\frac{1}{1-\alpha}}} \quad (8)$$

$\alpha$  is the parameter of the Eq. (1) [29]. When the volume resistance of a physical process is comparable to another physical process of the same material, then it will be also recorded in  $Z^*$  formalism (as a peak in  $Z''$  versus  $\log f$  diagram) with time constant  $\tau_Z (= 1/2\pi f_{\max, Z''})$  near the value  $\tau_M$ , but  $\tau_Z > \tau_M$ .

From Eqs. (7) and (8), it is evident that the activation energies of the same physical process, in various formalisms, will obtain the same values provided that the parameters  $\varepsilon_\infty$ ,  $\Delta \varepsilon'$ , and  $\alpha$  are not changed by temperature. Because such a behavior of the parameters  $\varepsilon_\infty$ ,  $\Delta \varepsilon'$ , and  $\alpha$  within a wide temperature range is not usual, the activation energies, like those that are calculated in various formalisms, are expected to have different values, for the same physical process.

In Fig. 9a, the Arrhenius diagrams of ionomer 30/70 regarding the MWS mechanism within  $\varepsilon^*$  formalism, and regarding the mechanism of high frequencies (h.f.) within formalisms  $Z^*$  and  $M^*$  are displayed. The parameter  $\beta$  of the fittings regarding Eq. (1) on the diagrams  $\log \varepsilon'$  versus  $\log f$  of 30/70 are generally characterized by values approaching unit. Therefore, the MWS mechanism will be effectively described by the equation Cole–Cole (Eq. (1),  $\beta = 1$ ). Specifically, at 353 K the parameters of Eq. (1), which characterize the MWS mechanism of 30/70, take the following values:  $\alpha = 0.13$ ,  $\beta = 0.95$ ,  $\Delta \varepsilon' = 15.5$  and  $f_0 = 7.7$  Hz with  $\varepsilon_\infty = 6.2$  at 500 kHz. From Eq. (8), it is estimated that the MWS mechanism will give maximum value  $M''_{\max}$  within formalism  $M^*$ , in frequency  $f_{\max, M''} = 32.5$  Hz. In the same temperature, the (h.f.) mechanism of  $M^*$  formalism gives maximum value  $M''_{\max}$  at frequency  $f_{\max, M''} = 39.7$  Hz. Therefore, the mechanism (h.f.) in  $M^*$  formalism corresponds to the MWS mechanism in  $\varepsilon^*$  formalism. In addition, as it is shown in Fig. 9a, in the respective temperatures, the frequencies  $f_{\max, M''}$  and  $f_{\max, Z''}$  regarding the (h.f.) mechanism in formalisms  $Z^*$  and  $M^*$  have almost equal values,

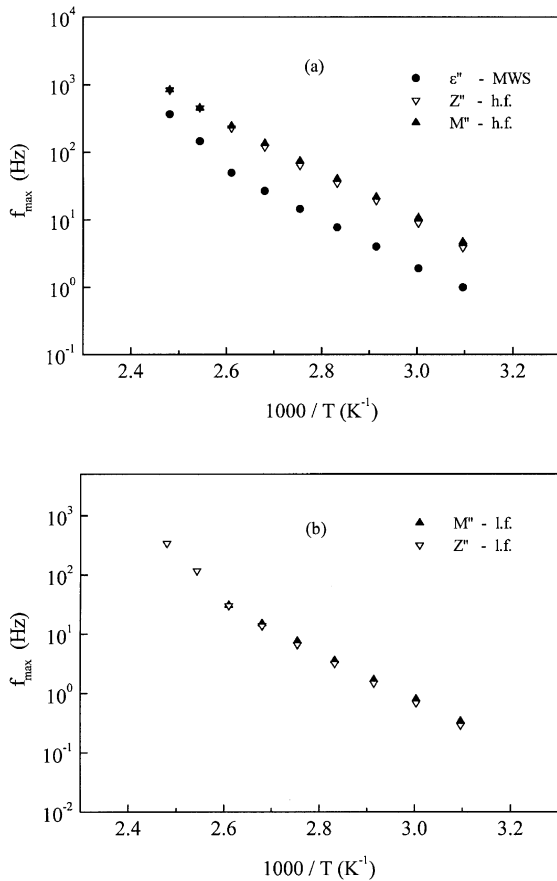


Fig. 9. Arrhenius diagrams of the ionomer 30/70 for the MWS mechanism ( $\epsilon^*$  formalism) and h.f. conductivity relaxation ( $Z^*$  and  $M^*$  formalism) (a). Arrhenius diagrams of the ionomer 30/70 for the l.f. conductivity relaxation in  $Z^*$  and  $M^*$  formalisms (b).

but  $f_{\max, M^*} > f_{\max, Z^*}$ . Thus, it is concluded that formalisms  $M^*$  and  $Z^*$  describe the same physical process and this physical process is correlated with conductivity relaxation mechanism, which is characterized by narrow distribution of relaxation times. Due to the fact that the MWS mechanism is correlated with charge migration within soft microphases, the (h.f.) mechanism in formalisms  $Z^*$  and  $M^*$  would correspond to the conductivity mechanism of the soft microregions.

In Fig. 9b, it is perceptible that the  $f_{\max, M^*}$  and  $f_{\max, Z^*}$  frequencies regarding (l.f.) mechanism of  $Z^*$  and  $M^*$  formalisms have almost equal values (but  $f_{\max, M^*} > f_{\max, Z^*}$ ). Therefore, the formalisms  $Z^*$  and

$M^*$  describe the same physical process and this physical process is correlated with conductivity relaxation mechanism, which is characterized by narrow distribution of relaxation times. The (l.f.) conductivity mechanism, as it has been already evidenced, is correlated with the hard microregions since it is systematically influenced more than the (h.f.) by the disordering (softening) of these regions. The respective diagrams of Fig. 9a,b regarding the other ionomers exhibit similar behavior.

From Eq. (5), it is evident that a conductivity mechanism, which is characterized by a high value volume capacity, will give a small magnitude  $M''_{\max}$  and vice versa. The (l.f.) conductivity mechanism of ionomers PU<sub>1</sub>/PU<sub>2</sub> is characterized by greater volume capacity in relation to the (h.f.) mechanism. Generally, this is to be expected, because the linear dimensions of hard microregions are smaller [19,31] than the respective ones of the soft microregions. Therefore, supposing that the prevalent conductive channels (regarding both hard and soft microregions) are directed towards the applied electric field, the (l.f.) conductivity mechanism, which is correlated with hard microregions, will be characterized by greater volume capacity in relation to the (h.f.) mechanism.

### 3.2.5. The dc conductivity

In Fig. 10, the dependence of the ac conductivity  $\sigma_{ac}$  ( $= 2\pi f\epsilon_0\epsilon''$ ) from the frequency  $f$  of the ap-

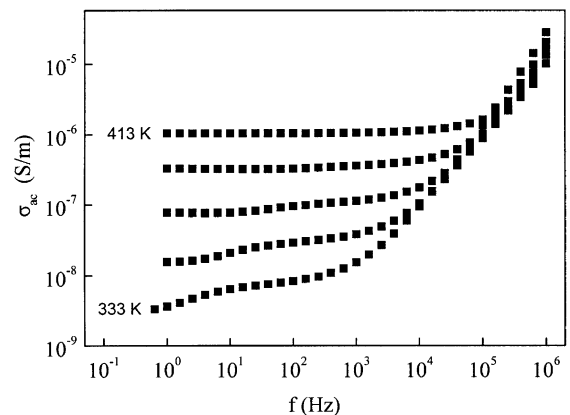


Fig. 10. Ac conductivity,  $\sigma_{ac}$ , versus frequency,  $f$ , for the 10/90 ionomer at several temperatures: 333, 343, 353, 363, 373, 383, 393, 403, 413 K.

plied electric field, regarding ionomer 10/90, at various temperature is displayed. From these diagrams, it is evident that  $\sigma_{ac}$  is independent of the frequency  $f$ , in a wide range of frequencies (in the region of low frequencies). This behavior is the same as the respective one of ‘pure’ dc conductivity. Nevertheless, in reality the slope of low frequency plateau, regarding diagrams  $\log \sigma_{ac}$  versus  $\log f$  (Fig. 10) do not reach zero. Due to temperature increase, the plateau is shifted to higher  $\sigma_{ac}$  values, as it is expected for thermal activated conductivity. The diagrams  $\log \sigma_{ac}$  versus  $\log f$  of the other ionomers PU<sub>1</sub>/PU<sub>2</sub> exhibit similar behavior form with that one of 10/90 shown in Fig. 10.

From the  $\sigma_{ac}$  values of the plateau, in the lower frequencies, we obtain the dc conductivity values,  $\sigma_{dc}$ , regarding the ionomers at various temperatures [32]. The  $\sigma_{dc}$  values, which have been obtained by using the above process, are in good agreement with those obtained by using a conductometer HP 4336 (high resistance).

The resistance  $R_{dc}$  can be estimated by the  $\sigma_{dc}$  values, using the equation  $R_{dc} = d/(S\sigma_{dc})$ , where  $d$  is the thickness of the samples and  $S$  the surface area of the electrodes. In Table 3a and b, the resistance values  $R_{dc}$  of ionomers PU<sub>1</sub>/PU<sub>2</sub>, which have been calculated by the plateau of diagrams  $\log \sigma_{ac}$  versus  $\log f$ , plots and also the resistance sums,  $R_h + R_1$ , of the two conductivity mechanisms, at respective temperatures, as they have been calculated by the best fits on the diagrams  $Z''$  versus  $\log f$  of Eq. (3) are shown. A very good agreement is observed between the values  $R_{dc}$  and  $R_h + R_1$ , which means that the two conductivity relaxation mechanisms (h.f.) and (l.f.) of the ionomers PU<sub>1</sub>/PU<sub>2</sub> correspond in series to the external electric stimulation within the complex impedance formalism  $Z^*$ .

### 3.2.6. The equivalent circuit of the two conductivity relaxation mechanisms

In the frequency region of (h.f.) and (l.f.) conductivity mechanisms, the equivalent circuit that depicts

Table 3

(a) The ( $R_h + R_1$ ) values ( $\times 10^6 \Omega$ ) of PU<sub>1</sub>/PU<sub>2</sub> ionomers, as estimated from the best fit of Eq. (3) to the  $Z''$  versus  $\log f$  diagrams, in various temperatures

$T$ (K)	100/0	50/50	30/70	10/90	5/95	0/100
413	37.9	–	–	1.6	7.7	–
403	146.9	1.4	4.7	2.6	16.2	–
393	476.7	2.4	8.7	5.1	37.4	0.13
383	1421.5	4.7	21.9	10.3	85.6	0.24
373	3857.5	9.8	49.8	21.7	190.1	0.62
363	–	21.5	104.9	48.8	406.2	1.8
353	–	49.2	223.4	108.3	831.0	5.6
343	–	102.2	443.9	248.5	1639.5	19.5
333	–	200.1	989.8	572.0	3203.1	64.5
323	–	449.4	2266.2	–	–	–

(b) The  $R_{dc}$  values ( $\times 10^6 \Omega$ ) of PU<sub>1</sub>/PU<sub>2</sub> ionomers, as estimated from the  $\log \sigma_{ac}$  versus  $\log f$  diagrams, in various temperatures

$T$ (K)	100/0	50/50	30/70	10/90	5/95	0/100
413	36.6	–	–	1.6	7.6	–
403	141.2	1.4	4.6	2.6	15.8	–
393	458.2	2.4	8.6	5.0	36.4	0.13
383	1375.5	4.8	21.3	10.1	83.3	0.24
373	3736.4	9.6	48.4	21.2	182.0	0.60
363	–	21.6	102.6	47.3	387.3	1.7
353	–	49.2	217.1	104.0	–	5.5
343	–	103.4	–	232.1	–	18.8
333	–	199.1	–	–	–	62.0
323	–	435.0	–	–	–	–

their response to the formalism  $Z^*$  is shown in Fig. 11a. This equivalent circuit (Fig. 11a) does not take into account the contributions of material–electrodes interfaces (which contribute within lower frequencies) and also the contributions of dipolar relaxation mechanisms (which contribute within higher frequencies, provided that  $R_h, R_l \gg R_{dip}$ ). Each conductivity mechanism is described by the parallel combination of a resistance ( $R_h, R_l$ ) and a constant phase element, CPE [26,27]. The complex impedance of the constant phase elements CPE is described by the equation  $Z_{CPE}^* = Z_0(i\omega)^{-(1-\alpha)}$ , where  $Z_0$  and  $\alpha$  are parameters, with  $0 \leq \alpha < 1$  [26,27]. The parameter  $\alpha$  is identical with the respective parameter  $\alpha$  of Eq. (3).

The parameters  $\alpha$  (Eq. (3)) of the two conductivity mechanisms, concerning temperatures higher than the respective temperatures of hard microregion dis-

ordering, take values within the region  $0 \leq \alpha < 0.1$ , in all PU<sub>1</sub>/PU<sub>2</sub> ionomers. In a first approach, it is reasonable to consider that the parameters  $\alpha$  of the conductivity mechanisms (l.f.) and (h.f.), at higher temperatures, take zero values. In this case, the equivalent circuit that describes the responsiveness of the two conductivity mechanisms of each PU<sub>1</sub>/PU<sub>2</sub> ionomer is depicted by the circuit in Fig. 11b, provided that the complex elements CPE<sub>1</sub> and CPE<sub>h</sub> are substituted by the pure capacities  $C_1$  and  $C_h$ , respectively. Thus, each conductivity mechanism is described by a single relaxation time ( $\tau_i = R_i C_i$ ).

The modified circuit ( $R_l C_l - R_h C_h$ ) of Fig. 11a corresponds to the response of such a system that consists of two layers of materials, parallel to the electrodes, having thickness  $d_1$  and  $d_h$ , dielectric constant  $\epsilon_1$  and  $\epsilon_h$  and specific resistance  $\rho_1$  and  $\rho_h$ , respectively, (Fig. 11b) [27]. The values of  $\rho_1$  and  $\rho_h$  are given by:

$$\rho_1 = R_l \frac{S}{d_1}, \quad \rho_h = R_h \frac{S}{d_h} \tag{9}$$

where  $R_l$  and  $R_h$  are the resistance values of conductivity mechanisms (l.f.) and (h.f.) of each ionomer, respectively.  $S$  is the surface area of electrodes between which is located the samples.  $d_1$  and  $d_h$  are the thickness of each layer regarding equivalent physical representation (Fig. 11b) of the modified equivalent circuit of Fig. 11a, with  $d_1 + d_h = d$ , where  $d$  is the thickness of the sample.

According to this two-layer model, the specific resistance  $\rho$  of each ionomer is described by:

$$R = R_l + R_h \Rightarrow \rho = \chi_l \rho_l + \chi_h \rho_h \tag{10}$$

where  $R$  is the resistance and  $\chi_l, \chi_h$  are the volume fractions of the total hard and soft regions of each PU<sub>1</sub>/PU<sub>2</sub> ionomer.

The respective capacities  $C_1$  and  $C_h$  of the two layers are described by:

$$C_1 = \epsilon_0 \epsilon_1 \frac{S}{d_1}, \quad C_h = \epsilon_0 \epsilon_h \frac{S}{d_h} \tag{11}$$

where  $\epsilon_0$  is the dielectric constant of empty space and  $\epsilon_1, \epsilon_h$  are the dielectric constants of each layer, respectively.

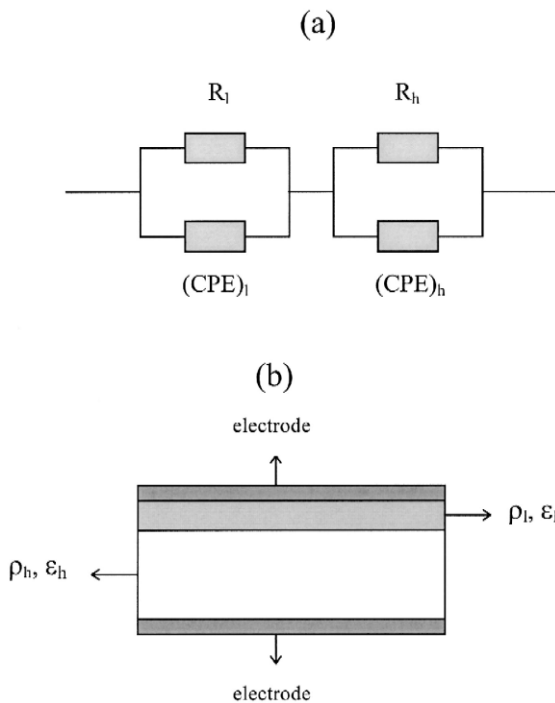


Fig. 11. The equivalent circuit which describes the responses of the two conductivity relaxations in  $Z^*$  formalism, at the respective frequency range (a). The physical representation of the previous equivalent circuit in the case where the complex elements CPE<sub>1</sub>, CPE<sub>h</sub> are the pure capacities  $C_1$  and  $C_h$ , respectively (the two layers Maxwell model) (b).

Assuming that the values of the dielectric constant of the layers do not differ significantly,  $\varepsilon_1 \approx \varepsilon_h$ , from Eq. (11) it is evident that:

$$\frac{C_1}{C_h} = \frac{d_h}{d_1}. \quad (12)$$

The relaxation time values of the conductivity mechanisms regarding the two layers with thickness  $d_1$  and  $d_h$ , are:

$$\tau_1 = R_1 C_1, \quad \tau_h = R_h C_h. \quad (13)$$

The values of the capacities  $C_1$  and  $C_h$  of the two layers, in the representation of the conductivity mechanisms of Fig. 11b, are calculated from Eq. (13). The necessary values of the parameters  $\tau_1$ ,  $R_1$ ,  $\tau_h$  and  $R_h$  concerning the conductivity mechanisms (l.f.) and (h.f.) calculated by the best fits of the Eq. (3) on the diagrams  $Z''$  versus  $\log f$  plots. Subsequently, using the values of the fraction  $d_h/d_1$  calculated from Eq. (12), the thickness of the two layers  $d_h$  and  $d_1$  ( $d_h + d_1 = d$ ) have been obtained. Finally, from Eq. (9), the specific resistances  $\rho_1$ ,  $\rho_h$  of the (l.f.) and (h.f.) conductivity mechanisms, in the physical representation of Fig. 11b, are calculated for each ionomer at the highest temperature region.

### 3.2.7. Micromorphological transitions

Fig. 12a,b gives the dependence of the specific resistances  $\rho_1$  and  $\rho_h$ , of each ionomer (at the highest temperature region, 373–413 K), as a function of the reciprocal temperature. As it is shown in Fig. 12a,b, the difference between the specific resistance  $\rho_1$  and  $\rho_h$  of 100/0—at a temperature region immediately following the disordering of its hard microregions—is significantly greater ( $\rho_1/\rho_h = 11–20$ ) in comparison to the respective differences of the other ionomers ( $\rho_1/\rho_h = 2–7$ ) at the same temperature region. By this result, it can be explained the fact that the contribution of the MWS mechanism, to the real part of dielectric function  $\varepsilon^*$ ,  $\Delta\varepsilon'$ , concerning ionomer 100/0, does not decrease immediately following the disordering of the hard microregions, as it occurs in the other ionomers (Fig. 5). When  $\rho_1$  takes greater than  $\rho_h$  value, the charges that concentrate on the SFT/STF interfaces practically do not discharge through the STF microregions. On the contrary, as soon as the parameters  $\rho_1$  and  $\rho_h$  be-

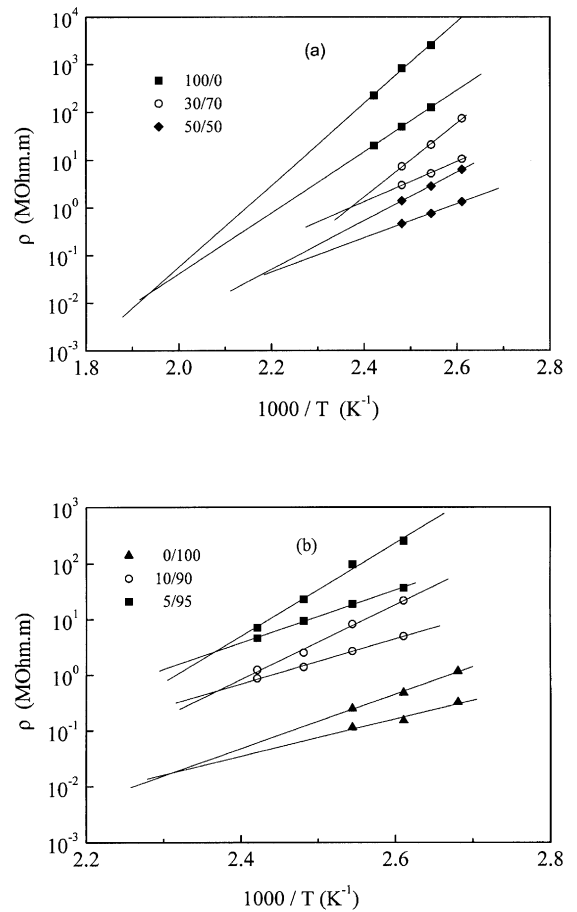


Fig. 12. The dependencies of the specific resistance  $\rho_1$  and  $\rho_h$  ( $\rho_1 > \rho_h$ ) from the inverse temperature, for all PU<sub>1</sub>/PU<sub>2</sub> ionomers, in the temperature range after the disordering of the hard microregions (a and b). The lines are the best fits of the Arrhenius type relation  $\rho = \rho_0 \exp(E_p/kT)$ .

come comparable (with each other), the discharge of these charges through the STF microregions is significant, and results in the decrease of the interfacial polarization which occurs between STF/SFT/STF interfaces, and thus in the decrease of the contribution  $\Delta\varepsilon'$  of the MWS mechanism.

In Fig. 12, the extrapolation plots of the best fittings of the Arrhenius equation  $\rho = \rho_0 \exp(E/kT)$ , and cross each other at the temperature region 420–512 K, is depicted. At the respective cross temperatures, specific resistances  $\rho_1$  and  $\rho_h$  have the same value. The existence of two different conductivity mechanisms, with the same resistance value  $\rho$ , does

not have any physical meaning [27]. The two conductivity mechanisms of each ionomer  $PU_1/PU_2$  at the respective cross temperatures,  $T_{MST}$ , become unified. The existence of two conductivity mechanisms in each ionomer  $PU_1/PU_2$  is correlated to the microphase separation. Thus, it is correlated to the appearance of discrete hard microregions dispersed within the soft phase. In the case of homogeneous materials, it is expected that there is only one conductivity mechanism. Thus, within each ionomer at the respective cross temperatures, a transition should occur from a micromorphological state characterized by separated microphases to a micromorphological state characterized by completely dispersed microphases. Microphase separation transition, MST, has been detected in non-ionic segmented polyurethanes, between 450 and 500 K, by the simultaneous use of DSC and SAXS methods [33].

The temperatures of the microphase separation transition,  $T_{MST}$ , of each ionomer are displayed in Table 4. From the values of Table 4, it is shown that the ionomer 100/0 has significantly greater  $T_{MST}$  than the other ionomers studied. As it has been immediately detected by the DSC thermograms obtained at 473 K (Fig. 1), all ionomers except 100/0 had been in liquid state. This fact probably implies that between 413 and 473 K, the hard microregions, which assured the good mechanical ionomer behavior, had been completely dissolved, resulting in a micromorphological homogeneity, i.e. in a complete microphase dispersion.

It is important to note that preliminary measurements on another similar system of ionomer blends  $PU_1/PU_2$ , in which the molecular weight (MW) of the  $PU_2$  (0/100) was greater (70 000–80 000) than the respective one of the above mentioned system (20 000–25 000), have shown that  $T_{MST}$  had been systemically higher, by 75–120 K, than the respective ones of the described system. This behavior does not seem to be dependent on the kind of the ionic

and effective groups of the  $PU_1$  and  $PU_2$  components, or on the degree of microphase separation (DMS) of the ionomers  $PU_1/PU_2$ , or on the differences in the weight fraction of the hard phase between the ionomers  $PU_1/PU_2$ . The significantly smaller  $T_{MST}$  of the  $PU_1/PU_2$  blends in relation to that of the 100/0 seems to be related with the smaller length of the macromolecules of the  $PU_2$  component. Smaller length of the macromolecules in one or both components of the  $PU_1/PU_2$  blends apparently seems to result in a shift of the microphase separation transition of the  $PU_1/PU_2$  ionomer blends to lower temperatures  $T_{MST}$ .

### 3.2.8. TSDC results in lower temperature region

In Fig. 13, a thermogram obtained by TSDC measurements of an ionomer blend with composition in  $PU_1/PU_2$  (%): 30/70 is shown. Four distinct dispersion regions corresponding to four dielectric mechanisms are observed.  $\gamma$ -relaxation at 121 K,  $\beta$ -relaxation at 160 K,  $\alpha$ -relaxation at 223 K, and Maxwell–Wagner–Sillars (MWS) relaxation at 254 K. Similar TSDC plots are obtained for all samples of the system studied. These four dispersions are observed in most polyurethane systems [20–22,34].

$\gamma$ - and  $\beta$ -relaxations are sub-glass secondary relaxations.  $\gamma$ -relaxation is associated to local motions of parts of the molecular chain [20–22,34].  $\beta$ -relaxation is attributed to the motions of the polar carbonyl groups of the polymer chains [20–22,34]. A systematic change of the magnitude (maximum of the current) and position (temperature of the maximum current) of these two relaxations dependent on the composition of the ionomers ( $PU_1\%$  content) has not been observed. The corresponding  $\beta$ - and  $\gamma$ -relaxation TSDC peaks appear at temperatures 160–168 and 116–124 K, respectively.  $\alpha$ -Relaxation is related to the reorientation of polar groups of the soft phase, during the glass transition of the soft microdomains [35]. MWS-relaxation is related to interfacial polar-

Table 4

The temperatures of the microphase separation transition,  $T_{MST}$ , of the  $PU_1/PU_2$  ionomers, as estimated by the use of the two layers Maxwell's model

$PU_1/PU_2$	100/0	50/50	30/70	10/90	5/95	0/100
$T_{MST}$ (K)	512 ( $\pm 12$ )	456 ( $\pm 8$ )	422 ( $\pm 5$ )	420 ( $\pm 5$ )	424 ( $\pm 5$ )	433 ( $\pm 5$ )

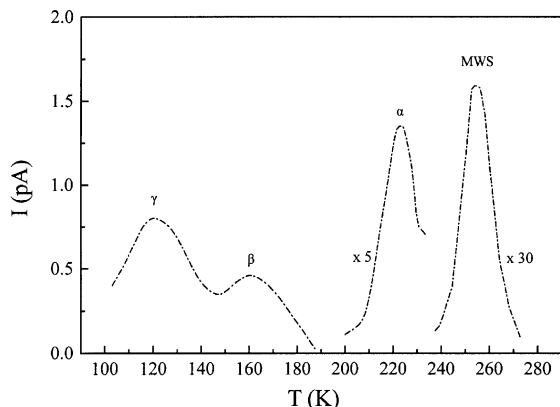


Fig. 13. TSDC thermogram for the  $PU_1/PU_2$ : 30/70 ionomer.

ization due to ion migration in the soft microregions and the existence of soft and hard microdomains with different conductivity [20–22].

Both  $\alpha$  and MWS-relaxations are strongly affected by the micromorphology of the materials. The temperature at which  $\alpha$  and MWS-relaxation appear in the TSDC plots and the magnitude of these relaxations are strongly affected by the degree of microphase segregation (DMS) of the ionomers [22]. In our previous work, based on TSDC measurements, a parameter,  $m_{TSDC}$ , as a criterion expressing the relative degree of phase mixing, was introduced [22]. SAXS measurements concerning DMS were in good agreement with the dielectric results and supported the criterion introduced for the relative degree of phase mixing based on dielectric TSDC measurements [22].

### 3.2.9. The correlation between the relaxation time of the MWS mechanism (AC) and the temperatures of the current peak maximum of the MWS and $\alpha$ mechanisms (TSDC)

In Fig. 14, an Arrhenius diagram of ionomer 30/70, in which the respective MWS peak point of the TSDC measurements ( $f_{1\sigma}$ ,  $1000/T_m$ ) is also included, is displayed representatively.  $T_m$  is the temperature of maximum current regarding MWS peak and  $f_{1\sigma}$  ( $=1/2\pi\tau$ ) is the equivalent frequency that corresponds to a relaxation time of about 100 s [22]. The very good linear relation (Arrhenius relation) between the points of the two methods (TSDC, AC) reveals that MWS mechanism is not directly related with motions of a large spatial scale

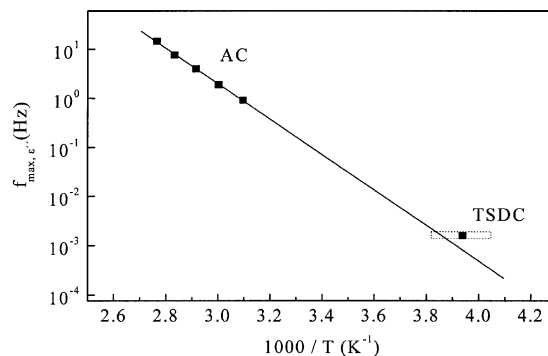


Fig. 14. Arrhenius plot of the 30/70 ionomer of the MWS mechanism (AC measurements), in which a point from TSDC measurements (details in the text) is included. The inverse temperature width that corresponds to the half height of the MWS current peak (TSDC) is also noted.

of the segments within the soft microphases ( $\alpha$ -relaxation obeys the non-linear VTF relation [36]). Similar linearity displays also the respective Arrhenius diagrams of the other ionomers. This fact probably implies that there is a low degree of interconnectivity between neighboring soft-rich microphases in  $PU_1/PU_2$  ionomer blends.

For a comparison of the results obtained by both methods, AC and TSDC, in Fig. 15 are shown the relaxation time  $\tau = 1/2\pi f_{max,c}$  at 353 K regarding the MWS mechanism of ionomers (AC measurements) and the difference  $\Delta T_1$  between the temperatures of the current maximum of MWS and  $\alpha$ -relaxa-

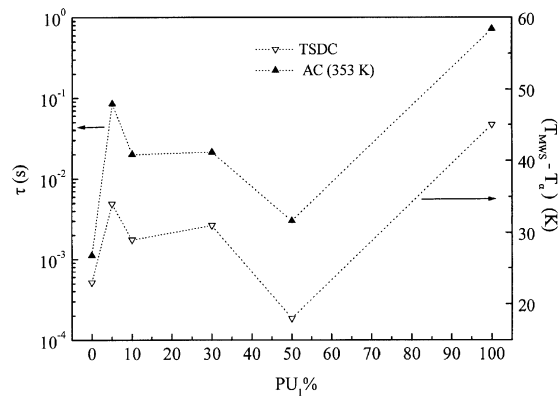


Fig. 15. The relaxation time,  $\tau$ , of the MWS mechanism at 353 K (AC measurements) and the difference  $\Delta T_1$  between the temperatures of the current maximum of the MWS and  $\alpha$ -relaxations, respectively,  $\Delta T_1 = T_{MWS} - T_{\alpha}$  (TSDC measurements), for all  $PU_1/PU_2$  ionomer blends.

tions, respectively,  $\Delta T_1 = T_{\text{MWS}} - T_\alpha$  (TDSC measurements). As it is observed in Fig. 15, the change of  $\tau$  among ionomers follows a respective change of  $\Delta T_1$ . The different incremental sequence of  $\tau$  values, in relation to the respective of  $\Delta T_1$  values, between 0/100 and 50/50 is attributed to the difference in activation energy between MWS mechanisms (Table 1) combined with the significant temperature difference of the measurement regions of the two methods. Thus, the difference  $\Delta T_1 = T_{\text{MWS}} - T_\alpha$  could be considered as a measure of the relaxation time  $\tau$  of MWS mechanism, specifically at a temperature region close to the respective MWS peak in the TDSC measurements.

The above result is in accordance to the third partial criterion for the degree of microphase separation which was introduced in our previous work [22]. The temperature of the current maximum for a depolarization peak in TSDC plots is related to the distance scale characterizing the movements of the relaxing units. MWS relaxation accompanies the glass transition during heating (depolarization) in TSDC measurements. This implies that the difference  $\Delta T_1 = T_{\text{MWS}} - T_\alpha$  could be considered as a measure of the distance scale for the movement of the charges accumulated at the soft/hard interfaces for their neutralization. Lower  $\Delta T_1$  would correspond to a lower distance scale and consequently to a smaller distance between hard phase–soft phase–hard phase interfaces. This implies lower degree of microphase separation or higher phase mixing, due to the broad distribution of size of the hard microdomains into the continuous soft phase [22]. Taking into account that the charge mobility of the PU<sub>1</sub>/PU<sub>2</sub> ionomers immediately after the glass-transition of the same soft phase is similar, it is expected that the time scale of the charge motion will be proportional to the distance scale of the charge motion between the nearest hard/soft/hard interfaces. Therefore, smaller  $\Delta T_1$  corresponds to a smaller relaxation time,  $\tau$ , of MWS mechanism.

### 3.2.10. Conductivity relaxation mechanisms and dc conductivity

In Fig. 16, the frequency of the maximum of  $Z''$ ,  $f_{\text{max},Z''}$  regarding the low frequency (l.f.) and high frequency (h.f.) conductivity relaxation mechanisms of all ionomers, at 373 K are shown in comparison.

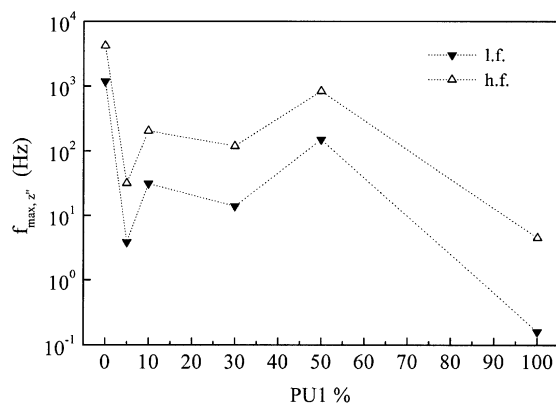


Fig. 16. The frequencies of the maximum  $Z''$ ,  $f_{\text{max},Z''}$ , of the l.f. and h.f. conductivity relaxations, at 373 K, for all PU<sub>1</sub>/PU<sub>2</sub> ionomer blends.

It is observed that a fast (h.f.) conductivity mechanism corresponds to a fast mechanism (l.f.) in the comparison between ionomers. This correlation between the relaxation time values  $\tau (= 1/2\pi f_{\text{max},Z''})$  of the two conductivity mechanisms can be explained in terms of concept of the dynamic energy barriers.

For instance, there are two ionomers A and B, where in A the relaxation time regarding the conductivity mechanism of soft microregions (h.f.),  $\tau_1$ , is smaller than the respective  $\tau_2$  of B. Assuming that the hard microregions of A and B correspond to a dynamic energy barrier with mean height  $W_{h1}$  and  $W_{h2}$ , respectively, which do not differ significantly,  $W_{h1} \approx W_{h2}$ .

Since  $\tau_1 < \tau_2$ , whereas the charges of B have not approached yet the bases of the barriers with height  $W_h$ , the charges of A remain at the respective bases (regarding electric modulation of the same duration). The possibility of a charge to pass in the unit of time,  $P_t$  (i.e the passage rate) through a dynamic barrier with height  $W_h$ , according to Boltzmann statistics is proportional to the term  $\exp(-W_h/kT)$ . Since the expectation time of charges, of ionomer A, at the bases of barriers with height  $W_h$  is greater than the respective one of B (by  $\Delta\tau = \tau_2 - \tau_1$ ), provided that  $W_{h1} \approx W_{h2}$ , the smaller  $\tau_1$  is in comparison to  $\tau_2$ , the greater is the  $P_t$  rate of A charges through the dynamic energy barriers, in relation to the respective rate of B. However, the inverse of  $P_t$  is the time constant (i.e the relaxation time) which

characterizes the conductivity mechanism that is related to the hard microregions. Therefore, the relaxation time of the conductivity mechanism, which is related to the hard microregions of A, will be also smaller than the respective one of B.

In Fig. 17a, the maximum frequencies  $f_{\max, \varepsilon''}$  of the MWS mechanism and the  $f_{\max, Z''}$  of the (h.f.) conductivity mechanism regarding all ionomers at 373 K are shown in comparison. It is observed that the  $f_{\max, Z''}$  change of the (h.f.) conductivity mechanism from one ionomer to another is followed by change of  $f_{\max, \varepsilon''}$  in the same direction. This is expected because the formalisms  $\varepsilon^*$  and  $Z^*$  describe the same physical process and therefore the respective characteristic relaxation time values will be proportional to each other.

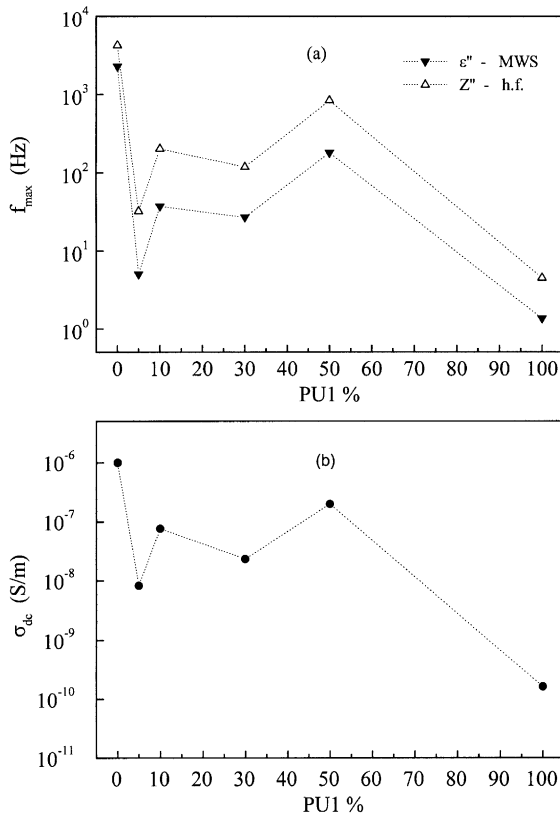


Fig. 17. The frequencies of the maximum  $\varepsilon''$  of the MWS mechanism,  $f_{\max, \varepsilon''}$ , and h.f. conductivity relaxation,  $f_{\max, Z''}$ , at 373 K, for all PU<sub>1</sub>/PU<sub>2</sub> ionomer blends (a). The dc conductivity,  $\sigma_{dc}$ , at 373 K, for all PU<sub>1</sub>/PU<sub>2</sub> ionomer blends (b).

As it has already been mentioned, the difference,  $\Delta T_1 = T_{\text{MWS}} - T_\alpha$ , where  $T_{\text{MWS}}$  and  $T_\alpha$  are temperatures of the current maximum regarding the peaks MWS and  $\alpha$ , respectively (in TSDC measurements), is a good measure of the relaxation time of the MWS mechanism,  $\tau = 1/f_{\max, \varepsilon''}$  (Fig. 15). Therefore, based on the above data, it is also a good measure of relaxation time of the (h.f.) conductivity mechanism,  $\tau = 1/f_{\max, Z''}$  at the temperature region before the disordering of the hard microregions. Thus, a smaller  $\Delta T_1$  (in a comparison between two ionomers) means a smaller relaxation time of the (h.f.) conductivity mechanism or equivalently a higher  $f_{\max, Z''}$ . Concurrently, a faster (h.f.) conductivity mechanism (in a comparison between two ionomers) means a faster (l.f.) conductivity mechanism as well (Fig. 16). Thus, the relaxation time values regarding both conductivity mechanisms will be proportional to  $\Delta T_1$ .

The temperature dependence of the dc conductivity,  $\sigma_{dc}$ , is given by the Nernst–Einstein relation  $\sigma(T) = q^2 n(T) D(T) / kT$ , where  $q$  is the charge of the ion carriers,  $n$  is the concentration of the ion carriers,  $D$  is the diffusion coefficient of the ion carriers,  $k$  is the Boltzmann constant and  $T$  is the absolute temperature. The diffusion coefficient,  $D$ , can be given by the relation  $D(T) = \lambda^2(T) / \tau(T)$ , where  $\lambda$  is the mean jump and  $\tau$  is the mean relaxation time of the ions hopping [37]. By combining the above relations, the temperature dependence of the dc conductivity can be given as follows:

$$\sigma(T) = \frac{q^2 \lambda^2(T) n(T)}{kT} \frac{1}{\tau(T)}. \quad (14)$$

Because of the strong temperature dependence of  $\tau$  (exponential dependence), it will be taken  $\sigma(T) \sim 1/\tau(T)$ , i.e. a faster conductivity relaxation mechanism means a higher contribution to the dc conductivity.

According to the Maxwell's model (two parallel layers model), the dc conductivity of each ionomer will be given as (relation (10)):

$$\sigma_{dc} = \frac{\sigma_1 \sigma_h}{\sigma_1 \chi_1 + \sigma_h \chi_h} \quad (15)$$

where  $\sigma_1$  and  $\sigma_h$  are the dc conductivities which correspond to the (l.f.) and (h.f.) conductivity relaxation mechanisms, respectively, and  $\chi_1$ ,  $\chi_h$  are the

volume fractions of the corresponding regions of the two conductivity mechanisms. In the temperature region before the disordering of the hard microdomains,  $(\sigma_h/\sigma_1) > 10$  for all PU<sub>1</sub>/PU<sub>2</sub> ionomers and also  $(\chi_h/\chi_1) \cong 2$ . Therefore, approximately, it will be  $\sigma_h \chi_h + \sigma_1 \chi_1 \cong \sigma_h \chi_h$  and consequently from the Eq. (15), it occurs that  $\sigma_{dc} \cong \sigma_1/\chi_h$ . Provided that  $\chi_h$  of the ionomers PU<sub>1</sub>/PU<sub>2</sub> differs less than 5%, the dc conductivity will be assessed exclusively by the contribution of the (l.f.) conductivity relaxation mechanism.

Taking into account the last three paragraphs, at a temperature region not much higher than the temperatures of the maximum current of the MWS mechanism (in TSDC thermograms), a smaller temperature difference  $\Delta T_1 = T_{MWS} - T_\alpha$  corresponds to a faster (h.f.) conductivity mechanism and also to a faster (l.f.) conductivity mechanism, and thus to greater values of  $\sigma_1$ ,  $\sigma_h$ , which means a greater value of dc conductivity,  $\sigma_{dc}$ .

In Fig. 17b, the conductivity  $\sigma_{dc}$  of all ionomers, at 373 K, is displayed. From the comparison between Fig. 17a and b, it is obvious that  $f_{max,e''}$  of MWS mechanism,  $f_{max,z''}$  of (h.f.) conductivity mechanism and  $\sigma_{dc}$  change precisely with the same sequence in ionomers PU<sub>1</sub>/PU<sub>2</sub>.

Therefore, the conclusion is that the temperature difference  $\Delta T_1 = T_{MWS} - T_\alpha$  is a reliable measure for comparing conductivity  $\sigma_{dc}$  of ionomers, at the temperature region above temperatures of the maximum current MWS peak and prior the disordering of the hard microdomains. The incremental sequence of  $\sigma_{dc}$  among ionomers is inversely correlated with the respective incremental sequence of  $\Delta T_1 = T_{MWS} - T_\alpha$ . At temperatures quite higher than  $T_{MWS}$ , significant differences in activation energies of MWS mechanisms are expected to alter the relative incremental sequence of ionomers  $\sigma_{dc}$ .

The ionomers 0/100 and 50/50, which exhibit the greater dc conductivity, are the ionomers which characterized by the smaller degree of microphase separation [22] and the smaller temperature difference  $\Delta T_1$ . However, the conductivity  $\sigma_{dc}$  does not seem to have any direct relation to the degree of microphases separation. This is because  $\Delta T_1$  is a parameter correlated with the broad distribution of size of hard microdomains, which is one of the factors that contribute to the mixing of the hard and

soft microphases [22]. Other factors are the dissolution of hard segments into the continuous soft phase, the existence of large dispersed boundary regions between soft and hard microdomains, and the existence of soft segments trapped in the hard microdomains. The conductivity  $\sigma_{dc}$ , as it has been shown above, is correlated directly to the temperature difference  $\Delta T_1 = T_{MWS} - T_\alpha$ .

#### 4. Conclusions

The ionomer systems PU<sub>1</sub>/PU<sub>2</sub> are characterized by the soft–hard microphase separation. The PU<sub>1</sub>/PU<sub>2</sub> ionomer blends are also characterized by the existence of two conductivity relaxation mechanisms. The analysis of the results, by using the formalism of the dielectric function,  $\epsilon^*$ , the complex impedance,  $Z^*$ , and the electric modulus  $M^*$ , reveals that the faster conductivity mechanism is related with the soft microregions, whereas the slower is related with the hard microregions. The comparison of the ionomers reveals that a faster conductivity mechanism of the soft microregions corresponds to a faster conductivity mechanism of hard microregions. The above mentioned behavior can be explained in terms of dynamic energy barriers.

According to our results, based on the measurements of AC dielectric spectroscopy and the Maxwell's model of two parallel to electrodes layers, at temperature region 420–456 K, a unification of the two conductivity mechanisms regarding all ionomers, except 100/0, should occur. This fact implies that at the respective temperature region, all ionomers (except 100/0) sustain a transition from a micromorphology characterized by a microphase separation to a micromorphology characterized by a complete microphase dispersion. DSC measurements, in the above respective temperature region, provide indications that the hard microregions had been dissolved into the soft phases. The respective temperature of micromorphological transition of 100/0 is rather higher, at 512 K. According to the DSC thermograms, there is no evidence for micromorphological transition of 100/0 ionomer up to 473 K.

There are indications that the temperature of micromorphological transition, regarding PU<sub>1</sub>/PU<sub>2</sub> ionomer blends, should be related directly with the

length of the macromolecules of the PU<sub>1</sub>, PU<sub>2</sub> components. A smaller length of the macromolecules, regarding one or both components of the PU<sub>1</sub>/PU<sub>2</sub> blends, should result in a shift of the microphase separation transition of the PU<sub>1</sub>/PU<sub>2</sub> ionomers blends to lower temperatures. This point needs further investigation.

The direct current conductivity,  $\sigma_{dc}$ , of the ionomers PU<sub>1</sub>/PU<sub>2</sub> is correlated directly with the temperature difference between the maximum of the MWS and  $\alpha$  peaks of the TSDC thermograms,  $\Delta T_1 = T_{MWS} - T_\alpha$ . A smaller difference  $\Delta T_1$  corresponds to a higher value of conductivity  $\sigma_{dc}$ . The temperature difference  $\Delta T_1$  seems to be a reliable criterion in order to compare the  $\sigma_{dc}$  conductivity among ionomers. At a temperature region not much higher than the respective MWS peaks, it is expected that  $\sigma_{dc}$  of ionomers increases according to the inverse increment sequence of  $\Delta T_1$ . The difference  $\Delta T_1$  could be considered as a measure of the distance scale for the movement of the charges accumulated at the soft/hard interfaces for their neutralization. Lower  $\Delta T_1$  would correspond to a lower distance scale and consequently, to a smaller distance between hard phase–soft phase–hard phase interfaces, which implies lower degree of microphase separation or higher phase mixing, due to the broad distribution of size of the hard microdomains into the continuous soft phase.

The formalisms of the dielectric function  $\epsilon^*$ , electric modulus  $M^*$ , and complex impedance  $Z^*$  of the AC dielectric spectroscopy, reveal the existence, with different weights, of the various mechanisms of dipolar and conductivity relaxations. The combined use of these three formalisms in complex materials, and especially their imaginary parts, gives the possibility to extract conclusions about the origin and the characteristics of the various relaxation mechanisms, as well as about the correlation of these relaxations with the physical processes which take place in the materials.

## References

- [1] C.W. Alice, W.J. Macknight, *Macromolecules* 29 (1996) 2421.
- [2] H. Chen, *Macromolecules* 29 (14) (1996) 4919.
- [3] L. Shaoxiang, E.M. Pearce, T.K. Kwei, *Polym. Prepr. (Am. Chem. Soc.)* 35 (2) (1994) 852.
- [4] K.H. Hsieh, L.M. Chou, S.S. Wong, *Angew. Makromol. Chem.* 168 (1989) 145.
- [5] M. Rutkowska, A. Eisenberg, *Macromolecules* 17 (1984) 821.
- [6] W.J. Macknight, T.R. Earnest, *J. Polym. Sci.: Macromol. Rev.* 16 (N1) (1981) 41.
- [7] M. Laleg, Y. Camberlin, *J. Macromol. Sci., Phys. B* 23 (2) (1984) 233.
- [8] C.G. Buzuin, A. Eisenberg, *Ind. Eng. Chem. Prod. Res. Dev.* 20 (N2) (1981) 271.
- [9] S. Chen, W. Chan, *J. Polym. Sci., Polym. Phys.* 28 (1990) 1499.
- [10] J.T. Koberstein, A.F. Galambos, L.M. Leung, *Macromolecules* 25 (1992) 6195.
- [11] S. Chen, W. Chan, *J. Polym. Sci., Polym. Phys.* 28 (1990) 1515.
- [12] Yu.S. Lipatov, V.V. Shilov, A. Bogdanovich, L.V. Karabanova, L.M. Sergeeva, *J. Polym. Sci., Part B: Polym. Phys.* 25 (1987) 43.
- [13] A.A. Brovko, L.M. Sergeeva, in: H.X. Xiao, K.S. Frish (Eds.), *Advances in Urethane Ionomers*, vol. 1, Tech. Publ., Lancaster, USA, 1995, p. 147.
- [14] E.F. Cassidy, H.X. Xiao, K.C. Frisch, *J. Polym. Sci., Polym. Chem. Ed.* 22 (N8) (1984) 1839.
- [15] P. Pissis, A. Anagnostopoulou-Konsta, D. Daoukaki-Diamanti, L. Apekis, C. Cristodoulides, *J. Non-Cryst. Solids* 131–133 (1991) 1174.
- [16] R.W. Seymour, S.L. Cooper, *J. Polym. Sci., Polym. Lett.* 9 (1971) 689.
- [17] R.W. Seymour, S.L. Cooper, *Macromolecules* 6 (1973) 48.
- [18] C. Yang, T.G. Grasel, J.L. Bell, R.A. Register, S.L. Cooper, *J. Polym. Sci., Polym. Phys.* 29 (1991) 581.
- [19] V.P. Privalko, E.S. Khaenko, A.P. Grekov, Yu.V. Savelyev, *Polymer* 35 (8) (1994) 1730.
- [20] G. Spathis, L. Apekis, P. Pissis, N. Ollivon, S. Quinquenet, *J. Macromol. Sci., Phys. B* 29 (1990) 31.
- [21] L. Apekis, P. Pissis, C. Christodoulides, G. Spathis, M. Niaounakis, E. Kontou, E. Schlosser, A. Shonhals, H. Goering, *Prog. Colloid Polym. Sci.* 90 (1992) 144.
- [22] C. Tsonos, L. Apekis, K. Viras, L. Stepanenko, L. Karabanova, L. Sergeeva, *J. Macromol. Sci., Phys. B* 39 (2) (2000) 155.
- [23] P.B. Macedo, C.T. Moynihan, R. Bose, *Phys. Chem. Glasses* 13 (6) (1972) 171.
- [24] K.A. Mauritz, *Macromolecules* 22 (1989) 4483.
- [25] C.J.F. Bottcher, P. Bordewijk, *Theory of Electric Polarization*, vol. II, Elsevier, Amsterdam, 1978.
- [26] K.S. Cole, R.H. Cole, *J. Chem. Phys.* 9 (1941) 341.
- [27] J.R. Macdonald, *Impedance Spectroscopy*. Wiley, New York, 1987.
- [28] V.D. Patton, C.C. Wang, S.A. Akbar, *J. Appl. Phys.* 78 (3) (1995) 1757.
- [29] R. Gerhardt, *J. Phys. Chem. Solids* 55 (12) (1994) 1491.
- [30] W. Cao, R. Gerhardt, *Sol. Stat. Ion.* 42 (1990) 213.

- [31] K. Imada, T. Miyakawa, J. Chatani, H. Tadokoro, *Die. Macromolek., Chem. B* 83 (1965) 113.
- [32] K. Funke, *Philos. Mag. A* 68 (4) (1993) 711.
- [33] L.M. Leung, J.T. Koberstein, *Macromolecules* 19 (1986) 706.
- [34] P. Hedvig, *Dielectric Spectroscopy of Polymers*. Adam Hilger, Bristol, 1977.
- [35] P. Pissis, L. Apekis, *J. Non-Cryst. Solids* 131–133 (1991) 95.
- [36] H. Vogel, *Phys. Z* 22 (1921) 645;  
G. Tamman, G. Hesse, *Anorg. Allerg. Chem.* 156 (1926) 245;  
G.S. Fulcher, *J. Am. Ceram. Soc.* 8 (1925) 339.
- [37] J.P. Crine, *IEEE Trans. Electr. Insul.* 26 (1991) 811.